Proceedings of ASME Turbo Expo 2011
GT2011
June 6-10, 2011, Vancouver, British Columbia, Canada

GT2011-45898

PRESSURE SIDE AND CUTBACK TRAILING EDGE FILM COOLING IN A LINEAR NOZZLE VANE CASCADE AT DIFFERENT MACH NUMBERS

Giovanna Barigozzi, Antonio Perdichizzi and Silvia Ravelli
Università degli Studi di Bergamo Dipartimento di Ingegneria Industriale
Viale Marconi 24044 Dalmine (BG) Italy Tel +39 0352052306 fax +39 035562779
giovanna.barigozzi@unibg.it, antonio.perdichizzi@unibg.it, silvia.ravelli@unibg.it

ABSTRACT

Tests on a specific designed linear nozzle guide vane cascade with trailing edge coolant ejection were carried out to investigate the influence of trailing edge bleeding on both aerodynamic and thermal performance. The cascade is composed of six vanes with a profile typical of a high pressure turbine stage. The trailing edge cooling features a pressure side cutback with film cooling slots, stiffened by evenly spaced ribs in an inline configuration. Cooling air is ejected not only through the slots but also through two rows of cooling holes placed on the pressure side, upstream of the cutback. The cascade was tested for different isentropic exit Mach numbers, ranging from M_{2is} = 0.2 to M_{2is} = 0.6, while varying the coolant to mainstream mass flow ratio *MFR* up to 2.8%. The momentum boundary layer behavior at a location close to the trailing edge, on the pressure side, was assessed by means of Laser Doppler measurements. Cases with and without coolant ejection allowed to identify the contribution of the coolant to the off the wall velocity profile. Thermochromic Liquid Crystals (TLC) were used to map adiabatic film cooling effectiveness on the pressure side cooled region. As expected, the cutback effect on cooling effectiveness, compared to the other cooling rows, was dominant.

NOMENCLATURE

c	blade chord
D	hole diameter
$DR = \rho_c/\rho_e$	density ratio
H	blade height
$H_{12}=\delta^*/\theta$	shape factor
$K = \frac{\nu}{U_e^2}\frac{dU_e}{ds}$	acceleration parameter
m	mass flow rate
M	Mach number
$MFR = m_c/m_e$	overall coolant to mainstream mass flow ratio
n,s	normal and parallel to the vane surface
$\mathrm{Re}_{2is} = U_{2is}c/\nu$	isentropic outlet Reynolds number
s	blade pitch
t	trench depth
T	temperature
$Tu_1 = \sqrt{\overline{u'^2}}/U_1$	inlet turbulence intensity
$U = \sqrt{u^2+v^2+w^2}$	local mean velocity
u,v,w	streamwise, transverse and spanwise velocity components
$VR = U_c/U_e$	velocity ratio
X,Y,Z	cascade coordinate system
α	injection angle
β	flow angle (axial direction)
δ	boundary layer thickness
δ^*	displacement thickness
$\eta = (T_{aw}-T_e)/(T_c-T_e)$	adiabatic film cooling effectiveness
ν	kinematic viscosity
θ	momentum thickness
ρ	flow density
$\zeta = (U_{2is}^2 - U_2^2)/\overline{\overline{U}}_{2is,ms}^2$	energy loss coefficient

Subscripts

1	inlet
2	exit
aw	adiabatic wall
c	cooling flow
e	free stream
is	isentropic condition
ms	at mid span
th	thermodynamic

Overbar

_	time averaged, pitch averaged
=	mass averaged, area averaged
‘	RMS

INTRODUCTION

The trailing edge cooling design of an airfoil results from a trade-off between aerodynamic efficiency, cooling effectiveness and manufacturing. Trailing edge cooling schemes should assure an adequate thermal protection of the blade, maintaining the trailing edge as thin as possible to increase the turbine efficiency. The trailing edge cutback can be a good solution: cutting material from the pressure side reduces trailing edge thickness and creates a slot from which air can emerge to shield the blade surface from the hot mainstream gas.

Many aspects concerning trailing edge cooling were studied in different flow regimes, spanning from aerodynamics and thermal performance to manufacturing issues. The focus of this work is to get a comprehensive characterization of a typical trailing edge cooling scheme by collecting both aerodynamic and thermal measurements. Previous studies dealing specifically with the pressure side cutback on a cascade model are not as numerous as expected. Very few of them managed both aerodynamic and thermal aspects. One of the most complete analyses was carried out by Ames et al. [1]. Their internal geometry consisted of an eight row converging pin fin array. They first focused on the aerodynamic penalty associated with the cutback (also called gill slot) trailing edge in a low speed cascade facility for different coolant discharge rates. Taking the solid vane as a reference, the cutback was found to increase the total pressure loss in the range of the coolant design flow rate. At flow rates greater than design, losses decrease while increasing coolant injection rates. This occurs when the coolant velocity exceeds the free stream local velocity so that the local flow is energized. Furthermore, they showed that the cutback is responsible for the thickening of the wake and for the intensification of the core loss associated with the passage vortex. In a companion paper [2], they also documented adiabatic effectiveness, η, distributions over a range of blowing ratios. Whatever the injection rate, the maximum η value of about 0.9 was maintained up to 3 cm downstream of the gill slot exit. Farther downstream, film cooling effectiveness starts decreasing and rapidly decays to values lower than 0.2 at the trailing edge. More recently, Fiala et al. [3,4] extended the investigation to a letterbox trailing edge configuration, which is formed by adding flow partitions to a pressure side cutback. Differences between solid vane, cutback vane and letterbox vane were compared providing evidence of both coolant ejection losses and film cooling effectiveness. The letterbox was found to have slightly reduced total pressure losses at a given coolant flow rate, compared with the gill slot, because of the smaller exit area. This implies that coolant is discharged with higher momentum causing a reduction in primary losses. Coherently, at flow rates greater than design, losses decreased with increasing coolant flow. However, the letterbox requires an increased pressure drop but authors did not evaluate thermodynamic losses. The advantage of using a letterbox did not emerge from thermal tests: near the slot exit, midline η distributions were similar in level to the cutback vane.

Otherwise, aerodynamic and thermal issues were faced separately. Starting from aerodynamics, several studies assessed the influence of cutback geometry and main flow conditions on discharge coefficients [5], total pressure losses [6], and thermodynamic losses [7,8] at different coolant flow rates. No study, to the authors' knowledge, combined boundary layer investigations with trailing edge cooling. Many basic studies dealing with the developing momentum boundary layer could be detailed, but none of them addressed the effects of coolant injection through the cutback on the boundary layer development along the pressure side of the airfoil. Several studies (see for example [9-11]) have shown that the boundary layers on the pressure side of a high pressure nozzle vane remain laminar in shape at low free stream turbulence conditions.

Shifting attention to thermal aspects, few other papers reported experimental investigations limited to film cooling effectiveness. Martini et al. [12] measured laterally averaged η downstream of their cutback trailing edge model, for three internal cooling configurations, at low mainstream velocity. Results indicated that the extension of the region having the highest η is strongly affected by the internal cooling scheme, whereas the decay of η further downstream is similar for all configurations. An explanation for this can be found in another paper by Martini et al. [13]: unsteady interaction between the mainstream and the coolant from the blunt cutback lip was considered responsible for the mixing process which ultimately affects film cooling. The continuation of this investigation was carried out by Horbach et al. [14]. They concentrated on external cooling performance of different internal pin fin configurations. Four different ratios of lip thickness to ejection slot height were investigated for a blowing ratio between 0.2 and 1.25. Lip thickness variations revealed strong influence on adiabatic film cooling effectiveness. An increase in lip thickness was found to intensify unsteady vortex shedding from the blunt lip, thus enhancing mixing of coolant with the mainstream. Kim et al. [15] measured adiabatic effectiveness in a test model resembling the trailing edge configuration of a first stage nozzle vane. The cooling scheme consisted of a discharge slot separated by partitions. Tests were conducted in a low speed tunnel for blowing ratios from 0.25 to 1. In an accelerating mainstream, film effectiveness showed a dependency on the blowing ratio, with an improved trend with increasing blowing ratio. Dannhauer [16] investigated two different cooling geometries of the pressure side trailing edge: the first one was equipped with a pressure side cutback while the second one had a row of cylindrical holes, upstream of the blade trailing edge. Tests were performed in a transonic linear cascade flow field with different coolant flow rates between 0.5% and 2%. In the first case, the separation of the main stream occurring on the pressure side, at the edge of the cutback, was correlated with the poor film coverage of the trailing edge region at the lowest coolant flow rate (0.5%). At higher *MFR* a more homogeneous distribution of the coolant was shown, with higher η values. It looked like that coolant refilled the separation region. A steady decay of film cooling efficiency was documented from the slot exit to the trailing edge. The intermediate coolant flow rate *MFR* = 1% was found to assure the best film coverage, except for the region near the exit of the cutback slots.

The influence of the outlet Mach number on aerodynamic and thermal aspects in a high pressure turbine cascade is discussed as a leading topic of this work. Within a National Research Project, experimental investigations were done to completely characterize trailing edge film cooling in a high pressure vane. A cooling configuration with a pressure side cutback and two cooling rows placed upstream of the cutback was chosen. The tested exit Mach numbers ranged from M_{2is} = 0.2 to M_{2is} = 0.6 while *MFR* was varied up to 2.8%. The present paper contributes to the existing body of literature in combining momentum boundary layer measurements with coolant ejection at a location close to the trailing edge. Other aerodynamic results for the same configuration can be found in a previous paper [17]. Local and laterally averaged distributions of adiabatic effectiveness over the pressure side cooled region are also documented. The sensitivity analysis, which is usually carried out by varying *MFR*, is extended to the exit Mach number.

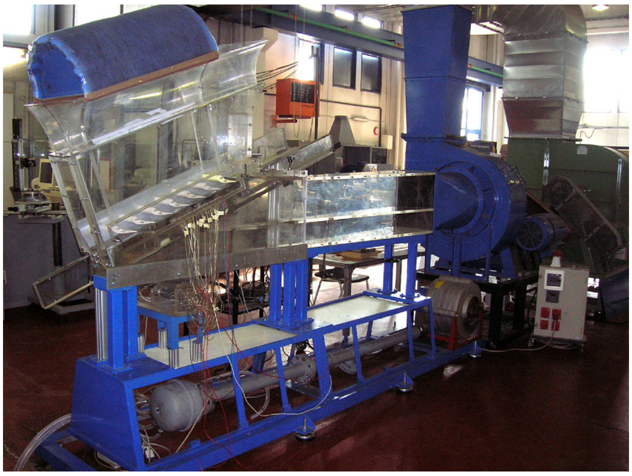

Fig. 1. View of the wind tunnel.

c = 142.1 mm	$\beta_1 = 90°$
$s/c = 1.04$	$\beta_2 = 20°$
$H = 98$ mm	M_{2is} = 0.2 - 0.6
$H/c = 0.69$	Re_{2is} = 6.5 10^5 - 1.6 10^6
$s_{TE} = 2.6$ mm	$Tu_1 = 1.6$ %
	$MFR = 0.0 – 2.8$ %

Table 1. Cascade geometry and operating conditions.

EXPERIMENTAL SETUP

The wind tunnel and the cascade model

Tests were performed in the subsonic wind tunnel for linear cascades at the Turbomachinery Laboratory of Bergamo University. This is a continuously operating, suction-type wind tunnel (Fig. 1). The side walls were constructed of Plexiglas for optical accessibility. The air blower, which is driven by a 125 kW electric motor, delivers a maximum isentropic Mach number M_{2is} = 0.7 at the cascade exit. A six-bladed linear turbine cascade was investigated. Details of cascade geometry are reported in Table 1 and Fig. 2. The blade profile imposes a design flow turning of 70°. The vane is characterized by a Zweifel coefficient of 1.18, indicating a highly loaded vane.

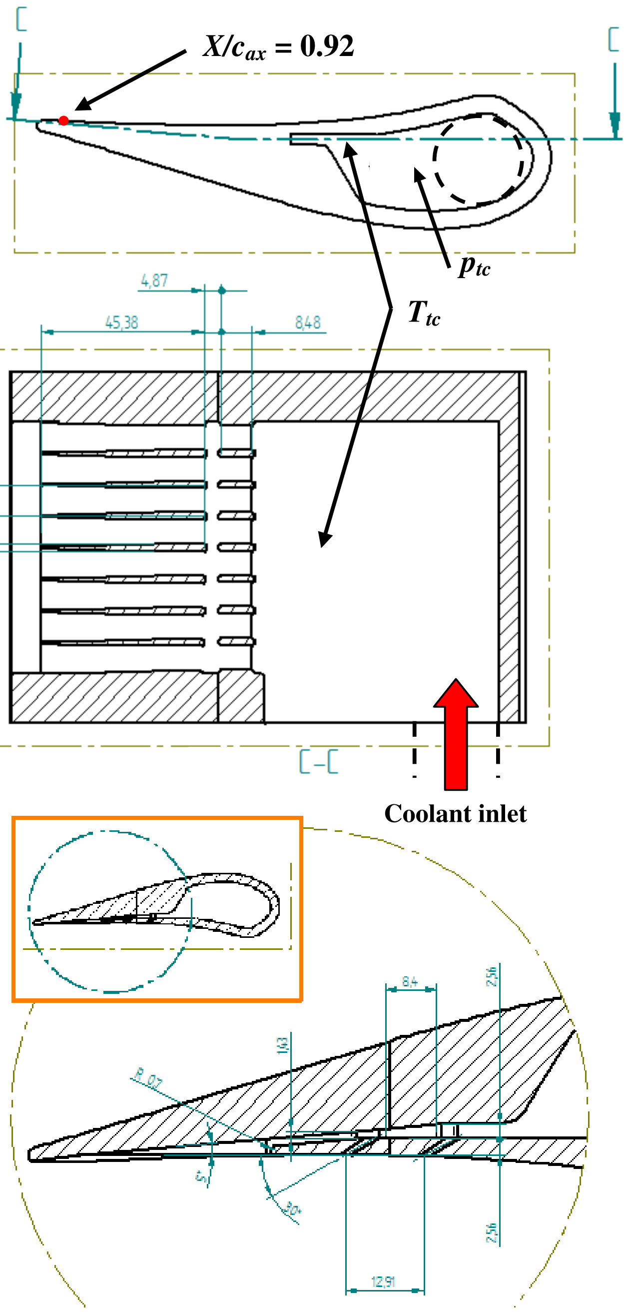

Fig. 2. Vane and trailing edge cooling geometry (size in mm).

A schematic of the cooled blade is shown in Fig. 2. The trailing edge of the three central vanes is equipped with two staggered rows of cylindrical holes and a cutback, all located on the pressure side. The first row is composed of 23 cooling holes and it is located at $X/c_{ax} = 0.52$. The second row is composed of 24 holes and it is located at $X/c_{ax} = 0.64$. Within each row, the hole-to-hole pitch is 2.76*D* and the hole length is 4.9*D*. The diameter of the cooling holes *D* is 1.1 mm. The holes are angled at 30° to the surface. Holes and cutback are spread over 70% of the blade height. The cutback starts at $X/c_{ax} = 70\%$. It consists of eight equally spaced rectangular slots. In order to increase the stiffness of the thin trailing edge and to enhance the internal heat transfer, an arrangement of rib arrays was adopted, as shown in Fig. 2. Coolant air is conveyed by a 3 kW radial fan to a plenum chamber, connected to the vanes by flexible ducts.

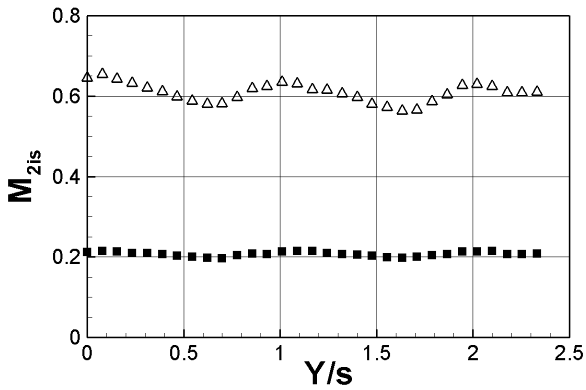

Fig. 3. Downstream M_{2is} distributions ($X/c_{ax} = 1.45$).

Testing Conditions and Measurements techniques

The cascade was tested at two different exit Mach numbers, i.e. $M_{2is} = 0.2$ and $M_{2is} = 0.6$, and at a low Tu_1 of 1.6%. Unfortunately the facility does not allow an independent variation of Reynolds and Mach numbers. It is worth pointing out that the blade was designed to work at $M_{2is} = 0.6$ and $Re_{2is} = 10^7$, meaning that the experimental setup exactly matches the real M_{2is} value but not Re_{2is} and Tu_1. In particular, much higher turbulence levels characterize the gas flow coming from the combustion chamber. But the influence of these parameters is significant only for the solid vane investigation. A higher Reynolds number in fact will in general anticipate transition [18,22]. Radomski and Thole [10] have shown that an increase of Tu_1 from 0.6% up to about 19% is responsible for the anticipation of boundary layer transition along the suction side, while on the pressure side the boundary layer still shows a laminar like behavior even if with increased velocity fluctuations and higher wall shear stress. This was due to the high acceleration that prevented transition. Similarly, in the present investigation, a higher Tu_1 value would anticipate transition on the solid vane suction side and probably modify the boundary layer behavior rear on the pressure side. A similar effect is expected due to the reduced Reynolds number. But when the vane pressure side is cooled, boundary layer behavior is completely dominated by coolant injection and cutback geometry, making the influence of Tu_1 and Re_{2is} of minor relevance.

Cascade operating conditions (Table 1) were controlled through a continuous monitoring of inlet total and static pressure and exit static pressure (31 wall taps located at $X/c_{ax} = 145\%$). Inlet total pressure and static pressure were measured by a three-hole probe in the admission section, about 1.6 c_{ax} upstream of the cascade inlet plane. In the same location the inlet boundary layer and the turbulence intensity were also measured using a flattened Pitot tube and a hot-wire probe. Flow periodicity was checked monitoring the cascade exit pitch wise pressure distribution by means of the aforementioned pressure taps distributed over the two central vane passages (Fig. 3). Finally, measurements of the solid vane profile pressure distribution were conducted substituting the two center vanes by instrumented ones equipped with 46 wall taps, distributed along the blade mid span. A HP 3852A D.A.C.U. unit (12 bit resolution) coupled with a 48 channels rotary pressure system (Scanivalve) were used to acquire all pressure data (± 100 mV range).

In the cooled configuration, *MFR* values up to about 2.8% were investigated. Injection conditions were controlled by monitoring the *MFR* and the coolant total pressure in the three vane feeding chambers. The injected mass flow was measured by an orifice device while coolant total pressure and temperature were measured by three pressure taps and three T-type thermocouples located on the vanes internal cavity (see Fig. 2). A maximum variation of ± 0.15% between the three coolant total pressures assured a good flow sharing between the three cooled vane and consequently a good periodicity. The uncertainty in the *MFR* value was calculated according to international standards for orifice devices [19]. δMFR resulted to be ± 0.04% at a value of $MFR = 0.5\%$ and ± 0.05% at a value of $MFR = 2.0\%$.

A 2D LDV system was used to study the momentum boundary layer behavior. The light source was a 300 mW Ar+ laser. A 200 mm focal length front lens allowed to measure a volume 0.06 mm in diameter and 0.6 mm in length. Two Burst Spectrum Analyzers were used to process the signals coming from the photomultipliers. All measurements were carried out acquiring 40000 burst signals at each location. Sawdust smoke was used to seed the flows, both main stream and coolant. The high number of acquired signals assured statistically accurate averages: based on a 95% confidence level, uncertainties of ±0.3% and ±0.8% for mean and RMS values, respectively, have been obtained for a turbulence intensity level of 23%. Boundary layer measurements were performed on the pressure side, at the $X/c_{ax} = 0.92$ location (Fig. 2). Results from other locations have already been discussed in a previous paper [17]. The traverse extended 3 mm perpendicularly to the blade surface and it was divided into 20 measuring points whose spacing was reduced down to 0.05 mm approaching the wall.

Sprayable wide banded Thermochromic Liquid Crystals (Hallcrest BM/R25C10WC17-10) were used to get the film cooling effectiveness distributions. TLC images were acquired by using a CCD camera, with a 767x573 pixels resolution. The primary lighting system consists of two 150 W white light sources, each one connected to two optical fibers. A TLC in situ calibration was performed on a flat plate since the curvature effects in the portion of the blade approaching the trailing edge are negligible. An aluminium plate was used for calibration and inserted inside the cascade test section in such a way to replace the central cooled vane. Both calibration and measurements were performed in the dark, in order to eliminate any influence of background illumination. Moreover, an illumination intensity as uniform as possible was provided to the model surface by properly orienting the lighting system, while simultaneously avoiding any light reflection onto the CCD camera. The light adjustment was performed with the vane model installed inside the test section and maintained also during calibration. A temperature gradient along the calibration plate was then generated by placing an electrical resistance on one side and a water cooled channel on the opposite side of the calibration device. This temperature gradient was captured by means of 10 T-type thermocouples installed just underneath the model surface. The whole calibration device was in turn previously calibrated using boiling water and melting ice.

During tests the heated secondary flow (DR = 0.95) was suddenly injected into the main flow at ambient temperature. The time history of the TLC image was recorded by the CCD camera, together with the temperature variation inside the feeding chamber. The RGB to hue conversion [20] was applied to the image data recorded after a time period in the range between 5 s and 10 s. Each image was selected in such a way to avoid important conduction phenomena in the most critical region, i.e. the lip just upstream of the cutback that is the thinner wall region (see Fig. 2). The time at which thermal conduction reached the external surface was in fact clearly detectable by looking at the recorded images. Please note that this instant always occurred after a stable temperature level inside the plenum was reached.

In the high M_{2is} case, film cooling effectiveness was calculated according to [21]. The usual free stream temperature was replaced by the recovery temperature T_r:

$$\eta = (T_{aw} - T_r)/(T_c - T_r) \qquad (1)$$

The recovery temperature was calculated from measured inlet cascade total temperature and solid vane profile isentropic Mach number distribution, assuming a minor influence of cooling system on vane loading. Moreover, the recovery factor was estimated from Prandtl number, assuming the main flow along the rear pressure side not so far from a turbulent boundary layer developing over an adiabatic flat plate [22].

The film cooling effectiveness measurement uncertainty depends on TLC and thermocouple measurements and conduction effects. In regions where conduction phenomena do not exist, the η uncertainty will range from ± 4.2 % with η = 0.8, up to about ± 15 % when η = 0.1. The 1D conduction correction proposed by Ethridge et al. [23] was applied to the recorded data in the region extending 1D just upstream of the cutback. A maximum correction of 0.10 was applied.

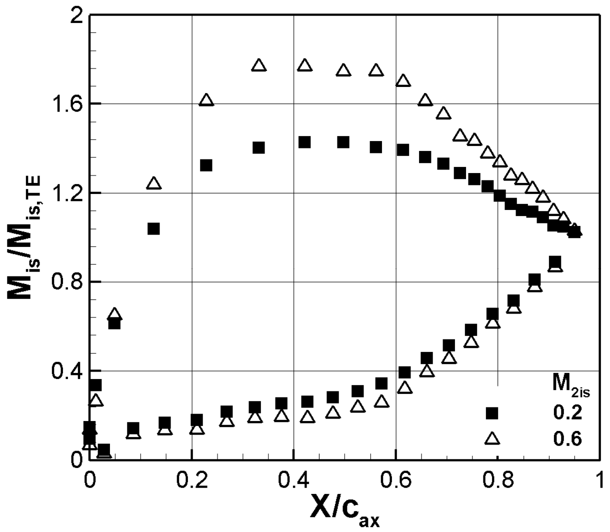

Fig. 4. Normalized isentropic profile Mach number distributions at Z/H = 0.5.

AERODYNAMIC RESULTS

After a characterization of the solid blade as a reference, attention will be drawn to the cooled vane. Performance of the cooling scheme will be assessed from the aerodynamic point of view, through discharge coefficients computation and boundary layer measurements.

Solid vane

The airfoil load measurements (Fig. 4) were performed through instrumented vanes at the mid span section, for the lowest and design exit Mach number. Results were plotted in terms of the ratio between the local Mach number and the one measured as close as possible to the trailing edge. The blunt leading edge is responsible for the strong acceleration up to almost 0.5c_{ax} along the suction side, followed by a strong diffusion up to the trailing edge. The maximum $M_{is}/M_{is,TE}$ value is about 1.8 on the suction side, at $X = 0.4c_{ax}$. No evidence of flow separation was observed, not even at the lowest tested Mach number. Along the pressure side, a moderate acceleration from the leading edge up to $0.4c_{ax}$ is followed by a much stronger acceleration up to the trailing edge. It should be considered that the first row of cooling holes is located in the region of moderate acceleration (X/c_{ax} = 0.52), while the second one (X/c_{ax} = 0.64) and the cutback (X/c_{ax} = 0.7) are located in the region of high acceleration. This, coupled with the presence of a unique plenum feeding both the cooling holes and the cutback, could negatively affect the injection condition through the first row of holes, at low injection rates. In fact, it may happen that the plenum total pressure is high enough to assure the cutback bleeding but too low to prevent main flow ingestion though the row of holes, causing a degradation in film coverage. Moreover, a much stronger acceleration takes place along the rear pressure side at high Mach number. Considering the region extending from cutback location up to the TE, the velocity gradient dU_e/ds almost triples when moving from M_{2is} = 0.2 up to 0.6, as shown by the acceleration parameter K distributions reported in Fig. 5.

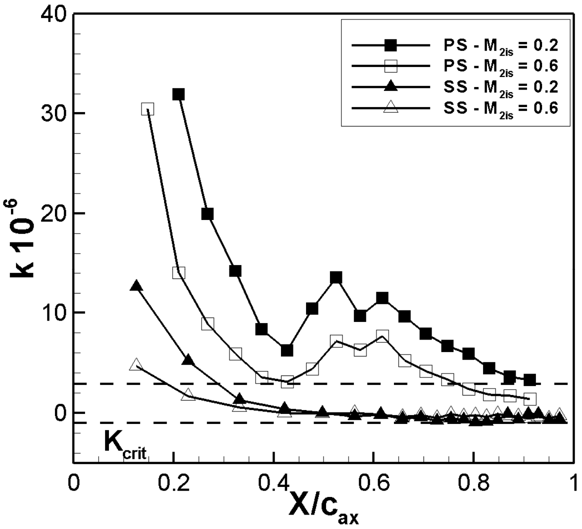

Fig. 5. Acceleration Parameter.

As well known, the most relevant parameters influencing boundary layer transition are the Reynolds number, the free stream turbulence level and the main flow pressure gradient, the latter well represented by the acceleration parameter K. The acceleration parameter was thus calculated from the profile Mach number distribution and compared against Mayle [24] transition criteria to analyze the influence of free stream velocity gradient on boundary layer development. These criteria define a critical K for transition and separation as a function of Tu (K_{crit} = -5.13 10^{-7} $Tu^{5/4}$) and a limiting value of $3 \cdot 10^{-6}$ for reverse transition. Notwithstanding the large diffusion on the suction side, especially at design Mach number, K is slightly negative but always higher than K_{crit}, indicating that no laminar separation would occur before transition. On the pressure side, at low Mach number, K is always larger than the limiting value of $3 \cdot 10^{-6}$, indicating that the boundary layer is expected to remain laminar up to the TE eventually going to transition in its very rear part. When Mach number increases, due to the increased vane loading the pressure side K distribution goes down, even below the limiting value. This means that the boundary layer can experience transition and become even turbulent before reaching the TE.

This behavior vs. Mach number is confirmed by boundary layer traverses performed $0.92c_{ax}$ downstream the leading edge (Fig. 6). In fact, mean and RMS velocity components show that the PS boundary layer is modified by the increased loading: its thickness almost doubles, both turbulence components increase, especially far from the wall and the shape factor reduces from about 2.10 at M_{2is} = 0.2 down to 1.54 at M_{2is} = 0.6. All these information allow to conclude that the PS boundary layer approaching the TE is laminar-like at low Mach number and is going to become turbulent at design operating condition.

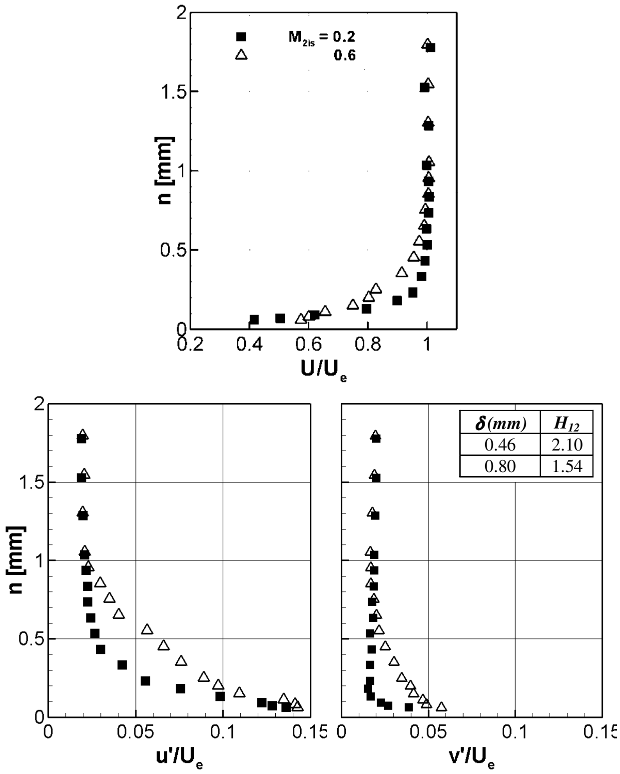

Fig. 6. Solid vane PS boundary layer traverses (X/c_{ax} = 0.92).

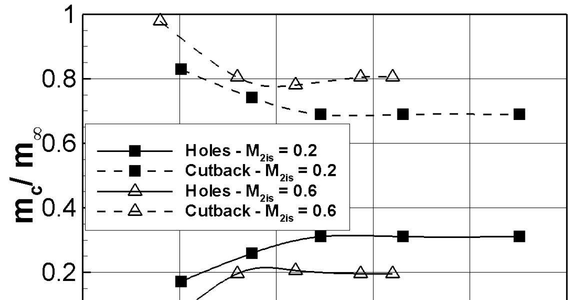

Fig. 7. Mass flow share between holes and cutback slots.

Cooling system characterization

Some preliminary tests were carried out on the cooled vane cascade to define the cooling system behavior. A first set of runs was performed with both holes and cutback blowing, by varying both the cascade operating condition (M_{2is} = 0.2 - 0.6) and the coolant to mainstream mass flow ratio MFR (0.0 – 2.8

%). The same tests were repeated with closed holes while the cutback was blowing. These data were used to define the mass flow sharing among holes and cutback. Figure 7 shows that most of the coolant exits through the cutback slots. The amount of coolant discharged through the holes decreases with rising M_{2is}, at constant *MFR*. This is consistent with the larger pressure decrease along the rear pressure side as well as with the increasing external cross flow influence; this is even more relevant at low pressure ratios.

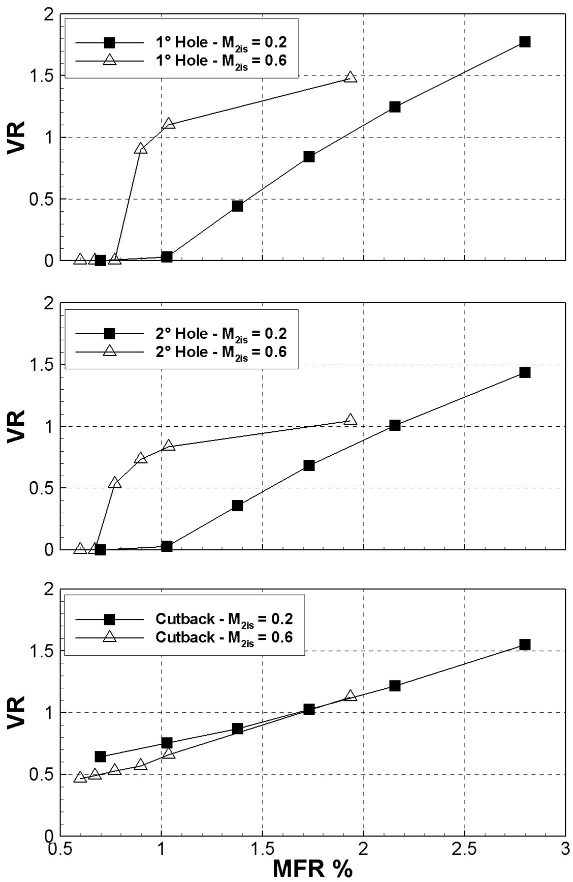

Fig. 8. *VR* for holes and cutback slots.

To fully characterize the injection system, discharge coefficients for holes and cutback were calculated independently. A unique discharge coefficient for all the holes was calculated, since it was a practical impossibility to perform tests without the cutback blowing and the mass flow through a single row is too small compared to the whole system blowing. To calculate the isentropic coolant mass flow rate, the exit isentropic Mach number for the holes was evaluated assuming a coolant isentropic expansion from internal blade cavity total pressure to hole exit static pressure. The hole exit static pressure was derived from the profile pressure distribution (Fig. 4), assuming that coolant injection does not significantly alter the solid vane load profile. Based on mass flow share and discharge coefficient values, holes and cutback coolant exit velocity were calculated and compared to the corresponding free stream velocity values. Figure 8 shows the obtained velocity ratio (*VR*) values at different injection conditions, for the two tested outlet Mach numbers. M_{2is} strongly influences the *VR* distributions, especially at the low *MFR*. This influence is much stronger for the two rows of holes than for the cutback. This is consistent with the much higher losses taking place inside the holes, especially at the low injection conditions. Worth to be noted is the *MFR* value for which *VR* becomes greater than unity: at the low Mach number it roughly corresponds to a *MFR* higher than 2.0 for both cutback and holes. When M_{2is} increases, the two rows of holes show increased *VR* values at low injection rates. Improved thermal performance at low injection rates are thus expected at design Mach number with respect to the low speed condition.

Boundary Layer characterization

Influence of coolant injection on the boundary layer behavior at the TE for variable downstream Mach number can be addressed by data in Figures 9 and 10. Mean and streamwise RMS velocity components at low M_{2is} and variable injection conditions are presented in Fig. 9 together with the ones of the solid vane case and cooled vane without blowing (*MFR* = 0.0%).

The cutback geometry appears to be responsible for a relevant boundary layer modification, approaching the TE. The boundary layer appears to be turbulent for all the tested *MFR* values, including the no blowing condition. The gradual increase in coolant injection from 1.0% to 2.8% causes a progressive re-energization of the boundary layer: in particular, an over speed at a distance from the wall between 0.5 and 1.5 mm is observed for the highest *MFR* value. As far as the streamwise turbulence component is concerned, the presence of the cutback strongly causes an increase in the u'/U_e values all over the boundary layer. For all the tested injection conditions, u'/U_e distributions show increased values at the wall, reduced values in the outer layer and slightly increased levels far from the wall, with respect to the no blowing condition (*MFR* = 0.0%). The distribution at *MFR* = 2.0% is quite similar to the one of the solid vane case. The trend of boundary layer modification vs. *MFR* is the result of the mixing process between coolant and main stream flow. Considering the case at *MFR* = 0.0% as a reference, the injection of a small amount of coolant (*MFR* = 1.0%) does not significantly alter the turbulence level close to the wall (n < 1 mm). With a further increase in *MFR* up to 2.0% the streamwise turbulence is reduced. This is the best interaction of mainstream and coolant flow with reduced mixing because the coolant is injected into the mainstream with a *VR* close to 1 (Fig. 8). With a further increase in *MFR* up to 2.8%, the coolant velocity gets higher than the mainstream one and the mixing process inevitably produces an increase in turbulence level.

Figure 10 compares boundary layer distributions for low and high velocity conditions at similar *MFR* values: 1.0% and 2.0%. When M_{2is} is increased up to 0.6, the boundary layer does not show significant modifications but for the region very close to the wall. For both the tested *MFR* values, reduced velocity defects and stream wise velocity fluctuations are noticeable, approaching the wall. As the boundary layer transition is surely triggered by coolant injection, the reduced turbulence close to the wall looks to be the result of a tendency of the turbulent boundary layer to re-laminarize downstream along the pressure side; this occurs because of the increased velocity gradient. Coolant exiting the slots probably remains confined at the wall, re-energizing the boundary layer even at the lowest tested *MFR* of 1.0%. This is consistent with the more favorable injection conditions taking place at design Mach number, as already evidenced by the velocity ratio data.

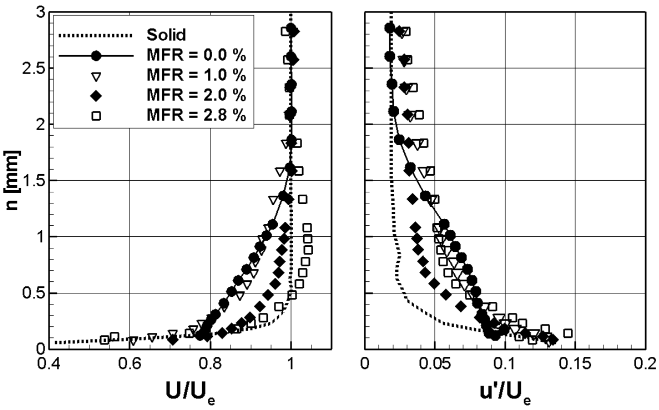

Fig. 9. PS boundary layer traverses (X/c_{ax} = 0.92) for variable *MFR* at M_{2is} = 0.2.

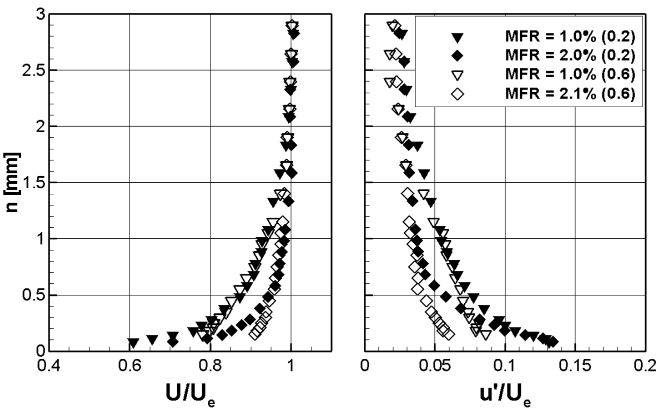

Fig. 10. PS boundary layer traverses (X/c_{ax} = 0.92) for variable *MFR* and M_{2is}.

THERMAL RESULTS

The capability of the cooling scheme to shield the trailing edge region from hot mainstream was evaluated by TLC measurements at the considered Mach numbers, for different *MFR* values.

Film cooling effectiveness

Adiabatic effectiveness contours on the cooled region of the vane at M_{2is} = 0.2 are presented in Fig. 11. A certain degree of non uniformity in the span wise direction can be observed. This is due to the fact that coolant is supplied only from one side of the vane (from the right in Fig. 11) and the inner plenum has a constant cross section along the vane span. Anyways, it clearly appears that cooling efficiency downstream of the cutback is promoted by increase in *MFR*. Thermal measurements at slot exits evidence higher η peak values, higher lateral spreading and increased persistency of the coolant when *MFR* grows from 0.8% to 2.8%. This agrees with open literature data [2,4,16], even if a direct comparison is difficult, due to the different cooling schemes. When coolant is injected with a small *MFR* (0.8% but also 1.2%), it is probably not distributed over the whole slot exit section, but it is mainly discharged from its most external portion, leaving the vane wall just downstream of the cutback practically uncooled. But as soon as it interacts with the external main flow, it is pushed down to the wall, resulting in the increased η values taking place at about s/c = 0.77. Further downstream, the low coolant momentum coupled with the high main stream acceleration produces the quick decay of thermal protection up to the trailing edge. A high level of cooling effectiveness in the area downstream of the cutback is obtained for *MFR* > 2%. In particular, the case with the highest *MFR* = 2.8% provides a high cooling efficiency also further downstream up to the trailing edge. The highest η values are now observed just downstream the cutback, indicating a good discharge condition for the slots.

Coolant injection from the two rows of holes do not follow the same trend. At the lowest *MFR*, i.e. 0.8%, no coolant exits the holes and even the cutback assures a very poor coverage just downstream of the slot exit. With a small increase in *MFR* up to 1.2%, coolant traces become evident at the exit of both the rows and η values downstream of the slots increases up to 0.7. For *MFR* greater than 2%, the first row of cooling holes does not work at all. Instead, the second one is found to work better at *MFR* = 2.1 than at *MFR* = 2.8%. This may be explained by considering the velocity ratio patterns of Figure 8. For the row #1, at $M_{2,is}$ = 0.2, a velocity ratio *VR* > 1 is reached when *MFR* > 1.9%. So, for *MFR* > 2%, coolant exiting from the first row is supposed to be detached from the vane surface. For row #2 coolant jets appear to lift off for *MFR* > 2.2%, that is the blowing condition corresponding to *VR* > 1.

Coolant persistence along the s/c coordinate can be better appreciated by computing laterally averaged η values (Fig. 12). These values were obtained by averaging η all over the span portion shown in Fig. 11 (0.15 < z/H < 0.85), thus, no correction aimed at excluding the rib region from the computation was implemented. Overall, the computed levels are in line with similar data available in the open literature [2,4,16]. It can be seen that increasing *MFR* is always worthwhile in the cutback region, but not downstream of hole rows. Downstream of row #1, the highest η_{av} level is reached for *MFR* = 1.2%. For the other blowing rates, one can note that thermal protection is practically absent after the first row, while after the second one an η_{av} between 0.15 and 0.2 is obtained.

Moving downstream, in the cutback region (s/c > 0.72), the coolant ejection effect on η_{av} becomes remarkable.

Similar patterns take place for all *MFR* values: η_{av} gets the peak close to the slot exit, then moving downstream, it starts to decrease up to the trailing edge. The effectiveness peak value grows from 0.2, at *MFR* = 0.8%, up to 0.75 occurring for the largest injection. The decreasing trend toward the trailing edge shows different slopes: the higher the *MFR*, the steeper the slope. Focusing on the trailing edge ($s/c = 1$), the maximum η_{av} value (about 0.3) was measured for *MFR* = 2.8%. Thermal coverage of this crucial area decreases progressively with a decrease in *MFR*.

The investigation at low Mach number showed that cooling holes and cutback injections provide the highest cooling effectiveness at different *MFR* values. This takes place also at the higher Mach number. Local distributions of η downstream of the cutback exit at M_{2is} = 0.6 are shown in Fig. 13, for *MFR* = 1.1 % and 2%. Results from measurements at *MFR* lower than 1% were not reported since thermal protection of the vane was very poor, as in the previous case.

The maximum tested *MFR* value of 2% is due to facility constraints occurring when it is operated at M_{2is} = 0.6. The contribution of the first row of holes to film cooling becomes negligible if *MFR* is raised above 2%. Conversely, film effectiveness downstream of the second row of holes improves by increasing *MFR*. Once again, velocity ratios of Fig. 8 may contribute in finding an explanation. In fact, at M_{2is} = 0.6, the threshold *MFR* values beyond which the velocity ratio exceeds 1 for the first and second row are about 1% and 2%, respectively. High levels of adiabatic effectiveness downstream of the cutback exit can be attained even at lowest *MFR*. Compared to the low velocity case, it can be deduced that at the higher Mach number a η improvement takes place both in lateral spreading and persistency. Note that at this higher Mach number (close to real engine operating conditions) with *MFR* = 2% the trailing edge gets a quite uniform thermal coverage with high η values (about 0.5).

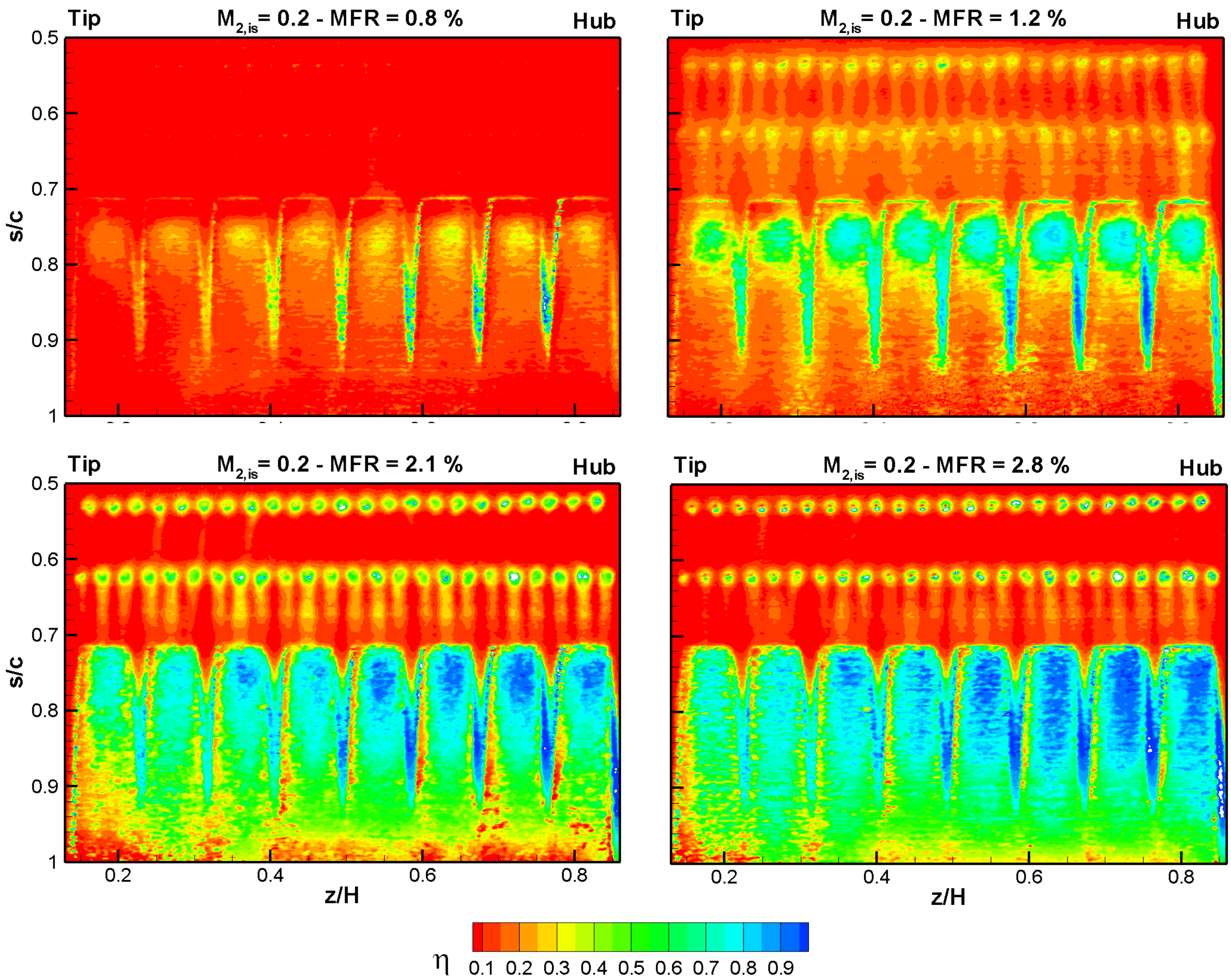

Fig. 11. Adiabatic effectiveness η for M_{2is} = 0.2 at different *MFR* values.

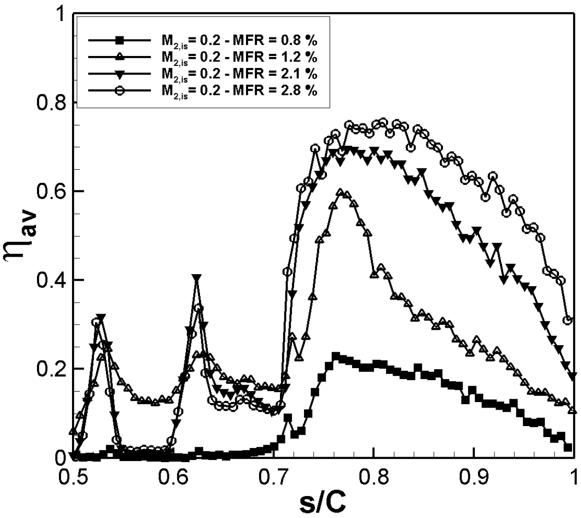

Fig. 12. Laterally averaged adiabatic effectiveness for M_{2is} = 0.2, at different *MFR* values.

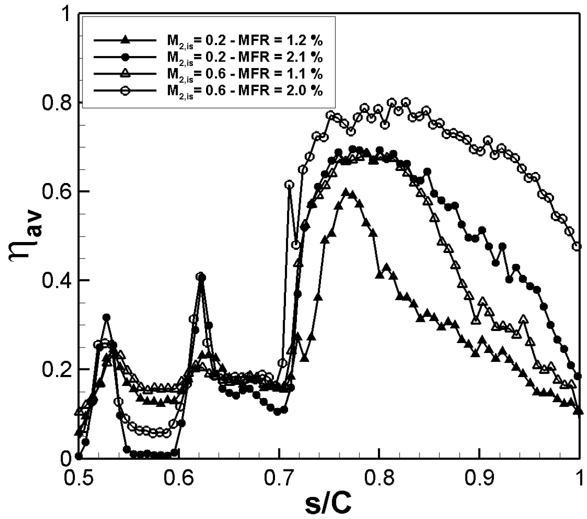

Fig. 14. Comparison between η_{av} for M_{2is} = 0.2 and M_{2is} = 0.6, at similar *MFR* values.

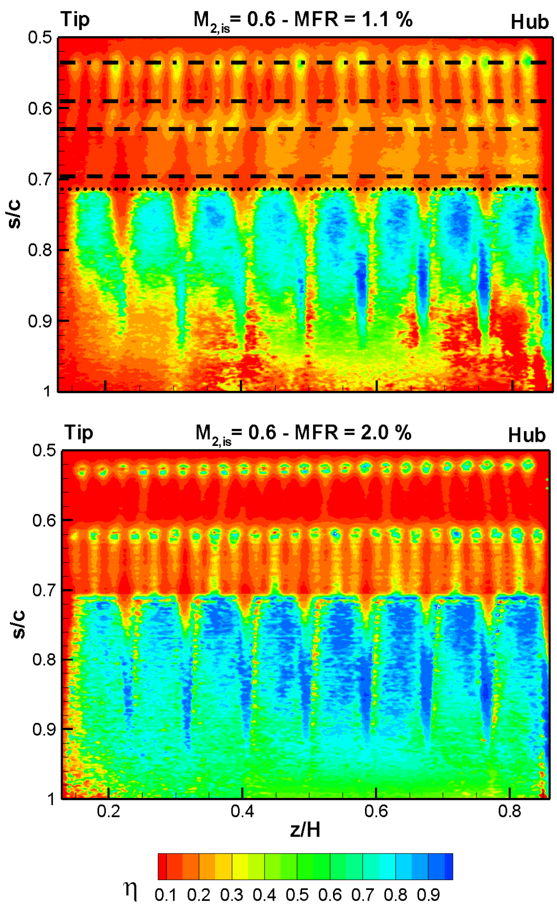

Fig. 13. Adiabatic effectiveness η for M_{2is} = 0.6 at different *MFR* values.

Laterally averaged adiabatic effectiveness are shown in Fig. 14. In order to put in evidence the effects related to M_{2is}, comparisons were carried out at similar *MFR* values. At the low injection condition, η_{av} improves by increasing M_{2is} from 0.2 to 0.6. This is evident in the area downstream of row #1, where the gain in η_{av} was slight, and in the cutback region, i.e. for *s/c* > 0.72, where a noteworthy enhancement of η_{av} can be noticed. Analogous conclusions can be deduced for the high injection condition, i.e. *MFR* = 2.0% – 2.1%. In this case, η_{av} augmentation due to the increase in M_{2is} is more consistent, not only downstream of row #1 but also in the cutback region. Here, moving downstream of the slot exit, the increment of η_{av} is progressively growing. This leads to a remarkable progress in thermal coverage at the trailing edge: in fact, η_{av} increases from 0.2 at M_{2is} = 0.2 to 0.48 at M_{2is} = 0.6.

Overall performance

Starting from the laterally averaged distributions, also an overall area averaged film cooling effectiveness value was calculated for each testing condition. The averaging process was split in three regions (see top of Fig. 13): the first one covers the vane surface extending from row #1 downstream edge up to about 2*D* upstream row #2 location. The second region covers the vane surface extending from row #2 downstream edge up to about $1D_{slot}$ upstream of the cutback (being D_{slot} the slot hydraulic diameter) and the last one extends from cutback up to the TE. Figure 15 reports the two holes and cutback area averaged data that substantially confirm the local and laterally averaged results. Higher area averaged film cooling effectiveness values characterize the high Mach number operating condition. This is particularly true downstream of the cutback slots. Here an almost constant effectiveness increase of about $\Delta\eta$ = 0.15 takes place for both

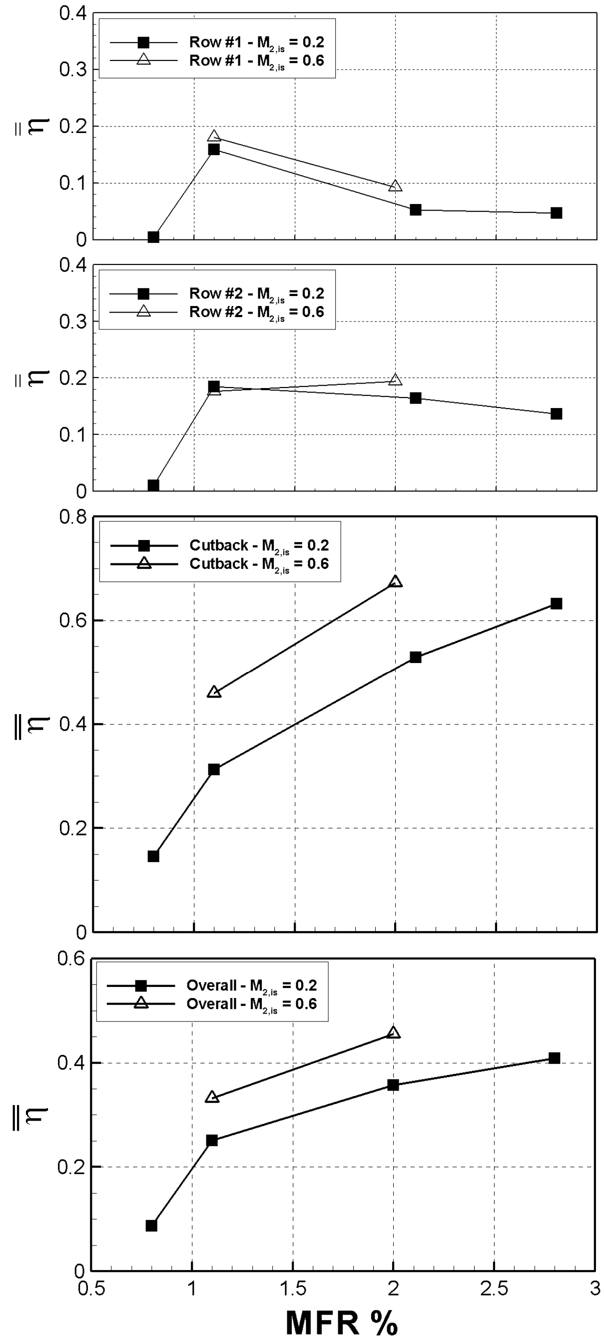

Fig. 15. Area averaged film cooling effectiveness for variable *MFR* and M_{2is}

tested *MFR* values. Film cooling effectiveness continuously increases with rising *MFR*, even if with a tendency to level off. At the highest tested *MFR* of 2.8%, for M_{2is} = 0.2 the effectiveness becomes larger than 0.6. An even larger value is reached when *MFR* = 2.0% and M_{2is} = 0.6. An optimal injection condition for row #1 takes place at *MFR* of about 1.0%, for both tested cascade operating conditions, with a slight improvement (about 13%) in the optimum value at M_{2is} = 0.6. Downstream row #2 similar results characterize the two tested operating conditions. Coolant injection with *MFR* of about 1.0 is still the best solution, giving an area averaged effectiveness of about 0.18.

Looking specifically at the cutback, results of Fig. 15 indicate that an improvement of trailing edge cooling effectiveness can be achieved by injecting increasing amounts of coolant. Finally, an overall area averaged film cooling effectiveness was also computed by averaging over the whole cooled vane surface (0.53 < *s/c* < 1.0). The cutback behavior dominates the overall thermal performance (bottom of Fig. 15), as the latter practically reproduces the cutback distribution but with reduced values: at M_{2is} = 0.6 and *MFR* = 2.0 %, the area averaged film cooling effectiveness is about 0.45.

The last goal of this work is to correlate results from the thermal analysis to the evaluation of the so called "thermodynamic" losses, in order to take into account the energy related to the injected flow.

Fig. 16 shows the comparison, in terms of profile (*2D*) and secondary thermodynamic (*Sec*) loss coefficients, between solid and cooled vane, for both exit Mach numbers. Secondary loss was obtained by subtracting the pitch wise averaged loss at mid span from the overall loss. As expected, profile losses increase with the injected coolant flow. However, coolant injection with *MFR* lower than 2.0% was responsible for a small increase in profile losses (+0.5%). In addition, profile losses reduce while increasing exit Mach number (-15%).

No influence of coolant injection on secondary losses was revealed: their value practically coincides with the one calculated for the solid vane, whatever the *MFR*. It follows that, whenever *MFR* is lower than 2%, thermodynamic penalties are not high enough to overshadow the advantage in thermal performance deriving from injecting large amounts of coolant.

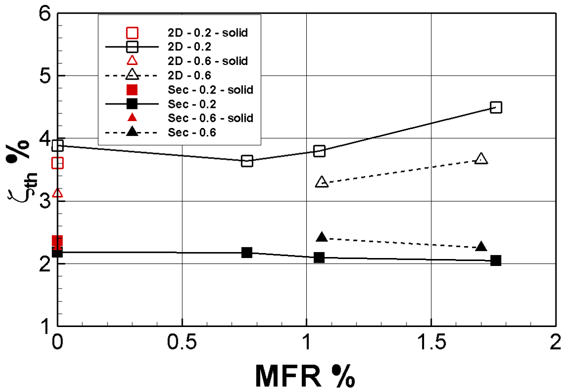

Fig. 16. Thermodynamic kinetic energy loss coefficient for variable *MFR* and M_{2is}.

CONCLUSIONS

A comprehensive experimental study was conducted on a linear nozzle vane cascade to characterize a trailing edge cooling scheme featuring a pressure side cutback, together with two rows of cooling holes. Tests were performed at two exit

Mach numbers by varying coolant flow rate up to *MFR* = 2.8%. The conclusions drawn from aerodynamic and thermal measurements are presented as following:

- More than 70% of the injected coolant flow exits through the cutback slots, whatever the *MFR*. An increase in M_{2is} further promotes the coolant discharge through the slots.
- The boundary layer behavior approaching the trailing edge does not show significant variations because of M_{2is}. Coolant exiting the slots remains confined to the wall and energizes the boundary layer.
- Adiabatic effectiveness measurements indicate that the region of highest film cooling efficiency is located at the slot exit. Its downstream extension increases with *MFR*.
- For both tested Mach numbers, cooling holes and cutback provide the best thermal coverage at different *MFR* values. Downstream of the cooling holes, the highest η_{av} level can be reached for *MFR* = 1.2%. Downstream of the slot exit up to the trailing edge, a gradual increase in *MFR* was found to improve cooling effectiveness.
- The gain in η_{av} due to outlet Mach number increase was particularly worthy downstream of the cutback, leading to a remarkable improvement in thermal coverage at the trailing edge. In this crucial area, the most efficient and homogeneous coolant distribution was obtained at M_{2is} = 0.6 and *MFR* = 2%.
- No significant increase in thermodynamic losses was found for *MFR* values lower than 2%. Within this range, the advantage in thermal performance is not overcome by thermodynamic penalties.

ACKNOWLEDGMENTS

The authors gratefully acknowledge the Italian Ministry of Instruction, University and Research (MIUR) for funding this research project. Authors are also grateful for the blade geometry provided by ALSTOM.

REFERENCES

[1] Ames F. E., Johnson J. D., Fiala N. J., 2007, Gill Slot Trailing Edge Aerodynamics - Effects of Blowing Rate, Reynolds Number and External Turbulence on Aerodynamics Losses and Pressure Distribution, ASME Paper GT2007-27399.

[2] Ames F. E., Fiala N. J., Johnson J. D., 2007, Gill Slot Trailing Edge Heat Transfer - Effects of Blowing Rate, Reynolds Number and External Turbulence on Heat Transfer and Film Cooling Effectiveness, ASME Paper GT2007-27397.

[3] Fiala N. J., Johnson J. D., Ames F. E., 2010, Aerodynamics of a Letterbox Trailing Edge: Effects of Blowing Rate, Reynolds Number, and External Turbulence on Aerodynamics Losses and Pressure Distribution, J. of Turbomachinery, v. 132, pp. 041011-1:11.

[4] Fiala N. J., Jaswal I., Ames F. E., 2010, Letterbox Trailing Edge heat Transfer: Effects of Blowing Rate, Reynolds Number, and External Turbulence on Heat Transfer and Film Cooling Effectiveness, *J. of Turbomachinery*, v. 132, pp. 011017-1:9.

[5] Uzol O., Camci C., Glezer B., 2001, Aerodynamic Loss Characteristics of a Turbine Blade with Trailing Edge Coolant Ejection: Part 1- Effect of Cut-Back Length, Spanwise Rib Spacing, Free-Stream Reynolds Number, and Chordwise Rib Length on Discharge Coefficients, *J. of Turbomachinery*, 123, 238-248.

[6] Uzol O., Camci C., 2001, Aerodynamic Loss Characteristics of a Turbine Blade with Trailing Edge Coolant Ejection: Part 2- External Aerodynamics, Total Pressure Losses, and Predictions, *J. of Turbomachinery*, 123, 249-257.

[7] Montis M., Niehuis R., Stephan B., 2009, Experimental Investigation of the Influence of Cooling Air Injection on the Aerodynamics of a High Pressure NGV-Cascade, Proc. 8th European Conference on Turbomachinery, 1301-1313.

[8] Rehder H. J., 2009, Investigation of Trailing Edge Cooling Concepts in a High Pressure Turbine Cascade-Aerodynamic Experiments and Loss Analysis, ASME Paper GT2009-59303.

[9] Bario F., Beral C., 1998, Boundary Layer Measurements on the Pressure and Suction Sides of a Turbine Inlet Guide Vane, *Exp Therm Fluid Sci*, 17, 1-9.

[10] Radomsky R., Thole K.A., 2002, Detailed Boundary Layer Measurements on a Turbine Stator Vane at Elevated Freestream Turbulence Levels, *J. of Turbomachinery*, 124, 107-118.

[11] Dees J. E. et al., 2010, Momentum and Thermal Boundary Layer Development on an Internally Cooled Turbine Vane, ASME Paper GT2010-23008.

[12] Martini P., Schulz A., Bauer H. J., 2005, Film Cooling Effectiveness and Heat Transfer on the Trailing Edge Cut-back of Gas Turbine Airfoils with Various Internal Cooling Designs, ASME Paper GT2005-68083.

[13] Martini P., Schulz A., Bauer H. J., Whitney C. F., 2005, Detached Eddy Simulation of Film Cooling Performance on the Trailing Edge Cut-back of Gas Turbine Airfoils, ASME Paper GT2005-68084.

[14] Horbach T., Schultz A., Bauer H. J., 2010, Trailing Edge Film Cooling of Gas Turbine Airfoils - External Cooling Performance of Various Internal Pin Fin Configurations", ASME Paper GT2010-23578.

[15] Kim Y. W., Coon C., Moon H. K., 2005, Film-Cooling characteristics of Pressure-Side Discharge Slots in an Accelerating Mainstream Flow, ASME Paper GT2005-69061.

[16] Dannhauer A., 2009, Investigation of Trailing Edge Cooling Concepts in a High Pressure Turbine Cascade – Analysis of the Adiabatic Film Cooling Effectiveness, ASME Paper GT2009-59343.

[17] Barigozzi G., Ravelli S., 2009, Effects of Trailing Edge Film Cooling on the Aerodynamic Performance of a

Nozzle Vane Cascade, Proc. 9th European Conference on Turbomachinery Fluid Dynamics and Thermodynamics.
[18] Drost U., Bölcs A., 1998, Investigation of Detailed Film Cooling Effectiveness and Heat Transfer Distributions on a Gas Turbine Airfoil, ASME Paper 98-GT-20.
[19] EN ISO 5167-2:2003(E).
[20] Camci C., Kim K., Hippensteele S.A., 1992, A New Hue Capturing Technique for the Quantitative Interpretation of Liquid Crystal Images Used in Convective Heat Transfer Studies, *J. of Turbomachinery*, 114, 765-775.
[21] Gritsch M., Schulz A., Wittig S., 1997, Adiabatic Wall Effectiveness Measurements of Film-Cooling Holes with Expanded Exits, ASME Paper 97-GT-164.
[22] Schlichting H., 1987, *Boundary Layer Theory*, McGraw-Hill.
[23] Ethridge M.I., Cutbirth J.M., Bogard D.G., 2001, Scaling of Performance for Varying Density Ratio Coolants on an Airfoil with Strong Curvature and Pressure Gradient Effects, *J. of Turbomachinery*, 123, 231-237.
[24] Mayle, R. E., 1991, The Role of Laminar-Turbulent Transition in Gas Turbine Engines, *J. of Turbomachinery*, 113, 509-532.